HHS Public Access

Author manuscript

Cancer Res. Author manuscript; available in PMC 2018 August 01.

Published in final edited form as:

Cancer Res. 2017 August 01; 77(15): 4158–4170. doi:10.1158/0008-5472.CAN-16-2212.

An immunosuppressive dendritic cell subset accumulates at secondary sites and promotes metastasis in pancreatic cancer

Justin A. Kenkel[1], **William W. Tseng**[1,2], **Matthew G. Davidson**[1], **Lorna L. Tolentino**[1], **Okmi Choi**[1], **Nupur Bhattacharya**[1], **E. Scott Seeley**[1], **Daniel A. Winer**[1,3], **Nathan E. Reticker-Flynn**[1], and **Edgar G. Engleman**[1]

[1]Department of Pathology, Stanford University School of Medicine, Palo Alto, CA 94304, USA

Abstract

Pancreatic ductal adenocarcinoma (PDAC) after complete surgical resection is often followed by distant metastatic relapse for reasons that remain unclear. In this study, we investigated how the immune response at secondary sites affects tumor spread in murine models of metastatic PDAC. Early metastases were associated with dense networks of $CD11b^{+}CD11c^{+}MHC\text{-}II^{+}CD24^{+}CD64^{low}F4/80^{low}$ dendritic cells (DC), which developed from monocytes in response to tumor-released GM-CSF. These cells uniquely expressed MGL2 and PD-L2 in the metastatic microenvironment and preferentially induced the expansion of T regulatory cells (Treg) in vitro and in vivo. Targeted depletion of this DC population in $Mgl2^{DTR}$ hosts activated cytotoxic lymphocytes, reduced Treg, and inhibited metastasis development. Moreover, blocking PD-L2 selectively activated CD8 T cells at secondary sites and suppressed metastasis, suggesting that the DC use this particular pathway to inhibit CD8 T cell-mediated tumor immunity. Phenotypically similar DC accumulated at primary and secondary sites in other models and in human PDAC. These studies suggest that a discrete DC subset both expands Treg and suppresses CD8 T cells to establish an immunosuppressive microenvironment conducive to metastasis formation. Therapeutic strategies to block the accumulation and immunosuppressive activity of such cells may help prevent PDAC progression and metastatic relapse after surgical resection.

Keywords

metastasis; tumor immunology; pancreatic cancer; dendritic cell; monocyte

Introduction

Pancreatic ductal adenocarcinoma (PDAC) is a particularly deadly form of cancer that often metastasizes to the liver or other organs before it is diagnosed, thereby eliminating the opportunity for surgical resection, which remains the only potentially curative treatment for

Corresponding Author: Edgar G. Engleman, M.D., Professor of Pathology and Medicine, Director, Stanford Blood Center, 3373 Hillview Ave., Stanford, CA 94304, Phone: 650-723-7960, Fax: 650-725-4462, edengleman@stanford.edu.

[2]Present address: Section of Surgical Oncology, Department of Surgery, University of Southern California, Keck School of Medicine, Los Angeles, CA 90033, USA

[3]Present address: Department of Pathology, University Health Network, University of Toronto, Toronto, ON M5G 2C4, Canada

Conflict of Interest: The authors disclose no potential conflicts of interest.

this disease (1, 2). Indeed, only ~20% of patients present with resectable tumors and unresectable PDAC is largely unresponsive to existing therapies, contributing to the dismal 5-year survival rate of around 5% (1, 2). However, even with surgery or effective control of local disease, survival rates remain low due to distant recurrence or metastasis progression (3-6), underscoring the need for new strategies to prevent and treat metastasis in this cancer.

Elements of the immune system have been shown to both prevent and promote tumor progression across a range of malignancies (7-10), and certain tumor immune profiles (e.g. low Treg, high CD8 T cell densities) are associated with favorable outcomes in human cancer (11, 12), including PDAC (13-15). In preclinical studies of PDAC, several myeloid and T cell populations have been shown to exacerbate disease and others to suppress it (16-25). Fewer studies, however, have specifically investigated the immune response at metastatic sites and whether it can be manipulated to suppress tumor spread (25-28). Considering the poor performance of immunotherapies tested to date in PDAC (29, 30), a better understanding of the tumor-associated immune response is critical for the development of more effective treatments.

Genetically engineered mouse models (GEMM) have greatly enhanced our understanding of PDAC initiation and progression (31, 32), helping to identify critical tumor-intrinsic as well as -extrinsic factors. The latter include various immune cells and mediators that operate in different ways and stages to support disease progression (16-25). However, while some PDAC GEMM eventually develop distant metastases, their highly variable rates and kinetics of metastasis preclude their use for a systematic study of the metastatic process. We recently developed an orthotopic mouse model of PDAC that resembles the human disease in its genetics, gross and microscopic appearance, and clinical manifestations (33). Most importantly, pancreatic tumors predictably metastasize to the liver in this immunocompetent model, permitting a systematic investigation of the metastasis-associated immune response. Recent studies have shown roles for different myeloid cell populations in metastatic seeding and outgrowth in various tumor models (7, 8, 34-36), but few have specifically investigated this process in PDAC (25-28). We therefore analyzed the livers of PDAC-bearing mice at early time points following tumor implantation to determine how the immune system affects metastasis development. Our results reveal a critical role for a phenotypically and functionally distinct population of dendritic cells (DC) in the spread of this intractable cancer.

Materials and Methods

Cell lines

The PDAC cell line, LMP, was established from liver metastases obtained from *Pdx1-Cre*; $Kras^{LSL\text{-}G12D/+}$; $Trp53^{LSL\text{-}R172H/+}$ mice on a B6/129 background, as described (33, 37). LMP cells stably labeled with tdTomato using a *Sleeping Beauty* transposon-based system were used for most experiments (38). PDA1-1 and PDA3-5 were established from primary tumors from *Pdx1-Cre*; $Kras^{LSL\text{-}G12D/+}$; $Trp53^{LSL\text{-}R172H/+}$ mice (33). The PDAC lines have been maintained in our lab since their establishment in 2008 and authenticated on the basis of mutant p53 expression by immunostaining. Panc02 and MC38 were obtained from the NCI DCTD tumor/cell line repository; and NIH/3T3, 4T1, B16-F10, CT26, and LLC from

ATCC between 2008 and 2014. All cell lines were frozen down at early passages (<5), routinely tested for mycoplasma contamination (Lonza MycoAlert), and used within 5 passages after thawing. Cells were routinely cultured in DMEM (Gibco) supplemented with 10% heat-inactivated FCS, 2 mM L-glutamine, 100 U/mL penicillin and 100 μg/mL streptomycin.

Mice

Six- to twelve-week-old B6129SF1/J (C57BL/6J × 129S1/SvImJ F1) mice were used as hosts in the LMP model unless otherwise indicated, and obtained from The Jackson Laboratory or bred in-house. C57BL/6J, *Csf2rb* KO, *Foxp3*^{DTR}, and B6.SJL-*Ptprc*^{a}*Pepc*^{b}/BoyJ (CD45.1) mice were obtained from Jackson and used for generating BM chimeras or crossed with 129S1/SvImJ mice to obtain tumor hosts. *Mgl2*^{DTR} mice on a C57BL/6 background (39) were crossed with 129S1/SvImJ mice to obtain tumor hosts. All procedures were approved by the Institutional Animal Care and Use Committee of Stanford University.

Tumor models

Orthotopic pancreatic tumors were established as previously described (33). Mice were injected in the pancreas with 2×10^5 tdTomato-labeled LMP tumor cells suspended in growth factor-reduced Matrigel (BD/Corning) and used 3-4.5 wk following tumor implantation unless otherwise indicated. Livers at this stage typically exhibited microscopic disease or small metastatic nodules. Normal livers were obtained from age-/sex-matched sham-operated or naïve mice. Details regarding tissue processing, cell isolation, and cell culture can be found in the Supplementary Materials and Methods. For experimental liver metastasis, mice were intrasplenically injected with 5×10^5 tumor cells in PBS and analyzed at the indicated time points. C57BL/6J mice were used for studies with B16, LLC, MC38, and Panc02 cells. Unless otherwise indicated, metastatic burden was measured by fluorescence emission using an in vivo imaging system (Xenogen IVIS). Liver lobes were imaged on both sides using a DsRed filter set, and average Total Efficiency values, which correct for nonuniformity in illumination, were used to assess metastatic burden.

Flow cytometry

Cell suspensions were Fc-blocked (clone 93, BioLegend) prior to incubation with fluorescently conjugated antibodies and LIVE/DEAD fixable dead cell stains (Life Technologies) for 20 min on ice. Intracellular staining was performed using buffers for Foxp3 staining (eBioscience). Antibodies were obtained from BioLegend, eBioscience, and BD Biosciences (see Supplementary Materials). Data were acquired on a BD LSR II flow cytometer and analyzed using FlowJo. After gating on live CD45$^+$ singlets, cell populations were defined as follows: PMN, CD11b$^+$Gr1^{hi}CD11c$^-$MHC-II$^-$SSC^{hi}; inf-Mo, CD11b$^+$Gr1^{int}CD11c$^-$MHC-II$^-$SSC^{lo}; CD11b$^+$ DC, CD11b$^+$CD11c^{hi}MHC-II^{hi}; CD11b$^-$ DC, CD11b$^-$CD11c^{hi}MHC-II^{hi}; KC/TAM, F4/80^{hi}CD11b^{int}; NK, NK1.1$^+$CD3$^-$; NKT, NK1.1$^+$CD3$^+$; CD4, NK1.1$^-$CD3/CD90.2$^+$CD4$^+$; CD8, NK1.1$^-$CD3/CD90.2$^+$CD8α$^+$; Treg, CD3/CD90.2$^+$CD4$^+$Foxp3$^+$.

Statistics

All statistical analyses were performed with GraphPad Prism. Unless otherwise indicated, two-tailed Student's *t*-tests were used to compare two groups, and one-way ANOVA with *post hoc* Tukey's tests for multiple comparisons. Mann-Whitney *U*-tests were used to compare non-normally distributed data where indicated, and medians are shown in the associated graphs. Values of $p < 0.05$ were considered significant.

Results

CD11b$^+$ DC accumulate at secondary sites and surround early metastases

Compared to tumor-naïve mice, CD11b$^+$ myeloid cells began to accumulate in the liver of orthotopic pancreatic tumor (LMP)-bearing mice as early as 2 weeks following tumor implantation and further increased in frequency by 3.5 weeks (Fig. 1A,C), at which point mice predictably exhibit microscopic disease or small metastatic nodules in this model (33). Consistent with reports in other models (7, 8, 34, 35), the CD11b$^+$ myeloid infiltrate included Gr1^{hi} (Ly6G$^+$Ly6C^{int}) neutrophils (PMN) and Gr1^{int} (Ly6G$^-$Ly6C^{hi}) inflammatory monocytes (inf-Mo) (Fig. 1B,C and Fig. S1A). These Gr1$^+$ cell populations, sometimes referred to as granulocytic and monocytic myeloid-derived suppressor cells (MDSC), respectively, have been the focus of many previous studies of myeloid cells in metastasis (24-26, 34, 35). We also observed a surprising increase in Gr1$^-$ (Ly6G$^-$Ly6C$^{-/lo}$) myeloid cells that expressed high levels of the dendritic cell (DC) markers CD11c and MHC-II (Fig. 1B,C). A similar myeloid infiltrate was noted during the development of lung metastases in mice with subcutaneous PDAC tumors, indicating that this response occurs at multiple metastatic sites in pancreatic cancer (Fig. S1B).

The abundant CD11b$^+$CD11c^{hi}MHC-II^{hi} population was distinct from liver-resident Kupffer cells (KC) and/or tumor-associated macrophages (TAM), which expressed lower levels of CD11b and higher levels of F4/80 and other macrophage (Mφ) markers (Fig. S1C,E). Indeed, similar to the CD11b$^-$CD11c^{hi}MHC-II^{hi} population, CD11b$^+$CD11c^{hi}MHC-II^{hi} cells in tumor-bearing mice expressed low levels of the Mφ markers F4/80 and CD64, and high levels of the DC marker CD24 (Fig. 1D and Fig. S1D) (40, 41). In contrast, F480^{hi}CD11b^{int} KC/TAM uniformly expressed CD64 but low levels of CD24 (Fig. S1E). CD103 was expressed by a small proportion of CD11b$^+$CD11c^{hi}MHC-II^{hi} cells but uniformly by the CD11b$^-$CD11c^{hi}MHC-II^{hi} population (Fig. 1D and Fig. S1D). These phenotypes are consistent with those described for CD11b$^+$ and CD11b$^-$CD103$^+$ conventional DC subsets in normal (40) and tumor (41, 42) tissues, and distinct from those described for F4/80$^+$CD24^{lo}CD64$^+$ Mφ /TAM (41). Thus, we will henceforth refer to the CD11b$^{+/-}$CD11c^{hi}MHC-II^{hi} populations as CD11b$^+$ and CD11b$^-$ DC.

The metastasis-associated myeloid subsets exhibited distinct microanatomical distributions. While CD11b$^+$ cells accumulated throughout the liver of tumor-bearing mice (Fig. S1F), micrometastases were typically bordered by dense networks of Gr1$^-$CD11c$^+$MHC-II$^+$ cells (Fig. 1E and Fig. S1G). In contrast, Gr1$^+$CD11c$^-$MHC-II$^-$ cells were more evenly dispersed in tissue sections and less enriched in and around early metastases (Fig. 1E). To compare the myeloid subsets on a functional level, we analyzed their cytokine secretion profiles and

found that CD11b$^+$ DC secreted the highest levels of most of the factors tested, including the protumoral mediators CCL2, CXCL1, CXCL2, IL-6, and TNFα (10, 43) (Fig. S1H).

CD11b$^+$ DC selectively expand at secondary sites and exhibit immunosuppressive features

These observations prompted a more thorough analysis of the liver DC compartment during metastasis development. As expected, there was a marked increase in total CD11c^{hi}MHC-II^{hi} DC in tumor-bearing mice, and the vast majority (~80%) of these cells also expressed CD11b (Fig. 2A). This contrasts with normal liver DC, which consist of roughly equal proportions of the CD11b$^+$ and CD11b$^-$ subsets (Fig. 2A). To assess potential functional differences among the DC populations, we analyzed the expression of various costimulatory/coinhibitory molecules and other maturation markers. DC from tumor-bearing mice expressed lower levels of CD86 and higher levels of CD80, ICOSL, PD-L1, and PD-L2 relative to normal liver DC (Fig. 2B). The selective expansion of CD11b$^+$ DC in tumor-bearing mice accounted for most of these changes, as these cells expressed less CD86 and more CD80, PD-L1, and PD-L2 relative to CD11b$^-$ DC (Fig. 2B,C). Both subsets expressed higher levels of ICOSL in tumor-bearing mice (Fig. 2B), while other maturation markers (4-1BBL, CCR7, CD40, RANK, OX40L) were minimally expressed under all conditions analyzed (data not shown). These data show that CD11b$^+$ DC richly associate with early metastases and express multiple immunosuppressive molecules and protumoral factors, suggesting that they may protect metastases from immune elimination and perform other protumoral functions. We thus decided to specifically study the ontogeny and function of this DC population.

Metastasis-associated CD11b$^+$ DC develop from monocytes in response to tumor-released GM-CSF

A large fraction of metastasis-associated CD11b$^+$ DC also expressed the monocyte/macrophage marker CD115 (M-CSFR) (Fig. 2B,C), suggesting that they could derive from monocytes (Mo). We tested this by adoptively transferring congenically marked (CD45.1) BM Mo from naïve mice into tumor-bearing mice. Prior to transfer, these cells expressed high levels of Gr1/Ly6C but not CD11c or MHC-II (Fig. 3A). However, when recovered from the liver after 5 d (Fig. 3B), more than 90% of the transferred cells expressed CD11c and MHC-II but not Gr1 (Fig. 3C,D), suggesting that Gr1$^+$/Ly6C$^+$ Mo predominantly differentiate into CD11b$^+$ DC at metastatic sites. Like host CD11b$^+$ DC, the vast majority of donor-derived CD11b$^+$CD11c$^+$MHC-II$^+$ cells expressed CD24 but not F4/80 or CD64 (Fig. S2A,B). Similar results were obtained at earlier time points post-transfer (d3; data not shown), suggesting that Mo directly traffic to and differentiate into CD11b$^+$ DC in the liver, although we cannot exclude the possibility of differentiation occurring elsewhere (e.g. primary tumor) prior to migration to the liver. We were unable to recover adequate numbers of cells for analysis from naïve mice (Fig. 3B), indicating that this recruitment and differentiation program is tumor-dependent. These results suggest that the large Gr1$^+$/Ly6C$^+$ Mo population in tumor-bearing hosts is a major source of metastasis-associated CD11b$^+$ DC, although we cannot exclude the involvement of other potential precursors such as CD11c$^+$Sirpα^{int} pre-cDC, which have been shown to develop into CD11b$^+$ DC in other tumor models (42). In light of previous studies showing that Gr1$^+$/Ly6C$^+$ Mo differentiate

into more Mφ-like cells (F4/80$^+$, CD64$^+$) in other models (35, 36, 42), our results suggest that Mo may exhibit a distinct differentiation pattern in PDAC.

To determine if tumor-derived factors can drive Mo to differentiate into CD11b$^+$ DC, we cultured BM Mo from naïve mice in the presence of tumor cell-conditioned medium (TCM) from the PDAC line (LMP) used throughout this study (33). LMP TCM treatment readily induced the formation of CD11c$^+$MHC-II$^+$ cells, while unconditioned or 3T3 fibroblast-conditioned media (3T3 CM) did not (Fig. 3E). Similar to metastasis-associated CD11b$^+$ DC, TCM-treated Mo also expressed high levels of CD80, PD-L1, and PD-L2 (Fig. 3F). DC differentiation was even more efficient when Mo were cocultured with LMP cells, with the majority of cells expressing CD11c and MHC-II after 2 days (Fig. S2C). PDAC cells have been reported to produce large amounts of GM-CSF (16, 17), which is routinely used to generate Mo-derived DC (Mo-DC). Consistent with this, we detected high levels of GM-CSF in LMP TCM but not 3T3 CM (Fig. S2D), and neutralizing GM-CSF inhibited DC differentiation and the upregulation of CD80, PD-L1, and PD-L2 in response to TCM treatment (Fig. 3G). To determine whether GM-CSF plays a role in CD11b$^+$ DC development *in vivo*, we generated BM chimeras with cells from WT (*Csf2rb*$^{+/+}$) or GM-CSFR KO (*Csf2rb*$^{-/-}$) mice, and used them as hosts in a model of experimental liver metastasis. Following intrasplenic (i.s.) injection of LMP cells, CD11b$^+$ DC accumulated in the liver of WT but not GM-CSFR KO BM chimeras (Fig. 3H). Moreover, metastasis was markedly reduced in the KO BM chimeras (Fig. 3I), reinforcing the pathophysiological function of GM-CSF in PDAC (16, 17).

Treg expansion supported by CD11b$^+$ DC facilitates metastasis development

These results collectively suggest that tumor-derived GM-CSF drives the accumulation of CD11b$^+$ DC with pro-metastatic functions. However, GM-CSF is a pleiotropic cytokine and has been shown to promote PDAC progression at the primary site through the expansion of Gr1$^+$ myeloid cells (16, 17), which is consistent with our data showing trends toward reduced Gr1$^+$ PMN and inf-Mo in GM-CSFR KO BM chimeras (Fig. 3H). We thus attempted to more specifically study the function of the metastasis-associated DC *in vitro* and *in vivo*. To this end, we examined the effects of DC from the liver of tumor-bearing mice (TLv-DC) on T cell responses in conventional *in vitro* assays. Contrary to expectations, TLv-DC more efficiently induced T cell proliferation in response to polyclonal (Fig. S3A) and antigen-specific (Fig. S3B) stimuli, as well as in mixed lymphocyte reactions (data not shown), compared to normal liver DC (NLv-DC). TLv-DC stimulated more IFNγ and IL-2 production under these conditions as well (Fig. S3C). Despite these data suggesting that metastasis-associated DC may be capable of inducing antitumor T cell responses, this did not occur *in vivo*. Instead, the accumulation of CD11b$^+$ DC in the liver was paralleled by an increase in Treg, with the frequency of Foxp3$^+$ CD4 T cells nearly tripling in micrometastatic liver (Fig. 4A). This was accompanied by a poor CD8 T cell response, leading to a doubling of the Treg:CD8 T cell ratio (Fig. 4A). We also observed a profound enrichment of Treg in the DC-rich areas bordering micrometastases, indicating that these cell populations interact *in vivo* (Fig. 4B). We detected a corresponding increase in Ki67$^+$ Treg (Fig. 4A) and colocalization of phosphorylated histone H3 and Foxp3 in DC-rich

perimetastatic tissues (Fig. S4A), suggesting that CD11b$^+$ DC may stimulate Treg proliferation *in situ*.

Consistent with the Treg-biased response observed *in vivo*, culturing syngeneic CD4 T cells with TLv-DC in the absence of additional stimuli led to a doubling of Foxp3$^+$ Treg compared to T cells cultured with NLv-DC or IL-2 alone (Fig. 4C). These results were largely attributable to the selective proliferation of Treg in coculture, with 70-80% of Treg undergoing cell division (Fig. 4C,D). Interestingly, Treg division rates were similar whether T cells were isolated from naïve or tumor-bearing mice, indicating that the T cell response does not depend upon prior tumor exposure (Fig. 4E). In contrast, TLv-DC poorly stimulated the proliferation of Foxp3$^-$ CD4 and CD8 T cells from tumor-bearing mice (Fig. 4F). Treg differentiation from naïve CD4 T cells or purified Foxp3$^-$ CD4 T cells (from *Foxp3^{GFP}* mice) was not induced under the same conditions (data not shown), suggesting that TLv-DC selectively expand pre-existing Treg. Correspondingly, neutralizing TGFβ, which is critical for the development of induced Treg (44), did not inhibit the Treg expansion but instead slightly enhanced it (Fig. S4B), and more than 80% of Treg in the liver of tumor-bearing mice expressed Helios (Fig. S4C), a putative marker of natural or thymic Treg (45).

Extending these results to more physiological settings, we observed spontaneous Treg proliferation when total non-parenchymal cells (NPC) from the livers of tumor-bearing mice (TLv-NPC) were cultured ex vivo in the absence of other stimuli (Fig. 4G and Fig. S4D). In contrast, Treg in cultures from naïve mice (NLv-NPC) exhibited poor survival and minimal proliferation (Fig. S4D). Treg proliferation was markedly reduced when TLv-NPC were depleted of either CD11b$^+$ or CD11c$^+$ cells, confirming a role for metastasis-associated CD11b$^+$ DC in this process (Fig. 4G). Furthermore, footpad injection of TLv-DC induced an expansion of Treg in draining compared to non-draining popliteal lymph nodes, demonstrating that these cells can expand Treg *in vivo* (Fig. 4H).

We next attempted to clarify the molecular mechanisms involved in the Treg expansion mediated by metastasis-associated DC. Blocking MHC-II largely abolished Treg proliferation (Fig. S4E), as well as the low level of proliferation among Foxp3$^-$ CD4 T cells, indicating a requirement for the presentation of tumor-derived or endogenous self peptides. Treg can proliferate in the absence of TCR-mediated signaling if provided with IL-2 and appropriate costimulation (46). Consistent with this, supplementing cultures with IL-2 partially rescued Treg proliferation under MHC-II blockade (Fig. S4F). The costimulatory requirements for Treg proliferation were determined by blocking molecules highly expressed by CD11b$^+$ DC. Blocking CD80 significantly inhibited the Treg expansion (Fig. S4G), and blocking ICOSL produced similar trends (data not shown). Surprisingly, antagonizing the PD-1 pathway with antibodies against PD-1, PD-L1, or PD-L2 failed to inhibit the Treg expansion in autologous pan T cell-DC cocultures from tumor-bearing mice and, instead, slightly enhanced it (Fig. S4H). However, blocking PD-1 signaling in this context also roughly doubled CD8 T cell division rates (Fig. S4I), suggesting that this pathway can still be targeted to improve CD8 T cell responses. Thus, metastasis-associated CD11b$^+$ DC preferentially stimulate Treg proliferation through the presentation of appropriate peptides and costimulatory molecules while suppressing CD8 T cell responses through the expression of PD-1 ligands.

These findings suggest that CD11b$^+$ DC may facilitate metastasis by both expanding Treg and suppressing cytotoxic T cells. To determine how the Treg response at secondary sites affects metastasis development, we used *Foxp3^{DTR}* mice as hosts in the orthotopic tumor model, allowing pancreatic tumors to grow for 3 wk before depleting Treg for 2 wk by weekly DT injections. Remarkably, the development of macroscopic liver metastases was nearly completely inhibited by Treg depletion despite the delayed depletion strategy (Fig. 4I). There was a trend toward smaller primary tumors in Treg-depleted mice (Fig. S4J), which could account for some of the reduction in metastatic burden. However, Treg depletion also markedly reduced metastasis following i.s. tumor cell injection (Fig. S4K). Although we cannot exclude a role for the system-wide immunostimulatory effects of Treg depletion in the results (47), these studies suggest that the Treg response supported by CD11b$^+$ DC at secondary sites facilitates metastasis development.

Selective depletion of CD11b$^+$ DC based on MGL2 expression enhances tumor immunity and inhibits metastasis

While seeking a way to specifically study metastasis-associated CD11b$^+$ DC *in vivo*, we discovered that most of these cells also expressed the C-type lectin MGL2 (CD301b) (Fig. 5A), which was recently shown to be expressed by CD11b$^+$ DC populations in multiple tissues (39, 48), including tumors (41). Importantly, MGL2 expression was almost completely restricted to CD11b$^+$ DC in the livers of tumor-bearing mice, with over 95% of MGL2$^+$ cells also expressing CD11b, CD11c, and MHC-II (Fig. 5B,C). Similar to the total CD11b$^+$ DC population, MGL2$^+$ cells also expressed high levels of CD24 but not CD64 or F4/80 (Fig. 5B and Fig. S5A). Furthermore, both spontaneous and experimental liver metastases were associated with dense networks of MGL2$^+$CD11c$^+$ cells (Fig. 5D and Fig. S5B). CD45.1$^+$ Mo transferred into tumor-bearing mice acquired high levels of MGL2 expression, with over 70% of donor-derived CD11b$^+$ DC expressing MGL2 (Fig. S5C). Moreover, TCM treatment of BM Mo induced the formation of MGL2$^+$CD11b$^+$ DC in a GM-CSF-dependent manner (Fig. S5D), suggesting that tumor-derived GM-CSF also drives the development of these cells. To determine whether MGL2$^+$CD11b$^+$ DC contribute to metastasis in other models, we analyzed the liver 2 wk following i.s. injection of B16, LLC, MC38, or LMP cells. Although all lines formed metastases, only LMP cells induced an accumulation of MGL2$^+$CD11b$^+$ DC (Fig. 5E). Consistent with a role for tumor-derived GM-CSF in the development of the DC, the other tumor lines produced low levels of GM-CSF compared to PDAC cells in vitro (Fig. 5F). Interestingly, like LMP, MC38 also induced an accumulation of CD11b$^+$CD11c^{hi}MHC-II^{hi} cells (Fig. S5E), but these cells expressed much lower levels of MGL2 compared to those elicited by LMP (Fig. S5F), suggesting that alternative factors drive the development of the CD11b$^+$ DC (or DC-like cells) in the MC38 model. Based on a recent study (42), these cells may differ in other ways from the CD11b$^+$ DC population in our model, including higher expression of the Mo/Mφ markers Ly6C and CD64.

To study the functional role of MGL2$^+$CD11b$^+$ DC in PDAC metastasis, we used mice that express DTR under the control of the endogenous *Mgl2* promoter as tumor hosts (*Mgl2^{DTR}*) (39). We examined the effects of MGL2$^+$ cell depletion in the experimental metastasis model, since MGL2$^+$CD11b$^+$ DC also accumulated at the primary site in the orthotopic

model, albeit at lower frequencies compared to the liver (Fig. S5G). DT treatment effectively depleted MGL2$^+$ DC in tumor-bearing mice, reducing their frequency to <1% of liver NPC (Fig. 5G). MGL2$^+$ cell depletion beginning 10 d after tumor injection led to a marked reduction in metastatic burden (Fig. 5H), indicating an overall protumoral function for this DC population. Given their immunosuppressive features, we hypothesized that MGL2$^+$ DC depletion reduces metastasis by removing restraints on antitumor immune responses. We tested this by examining the effects of cell depletion on the immune response to established metastases, allowing metastases to develop for 20 d before treating with DT or PBS for 5 d. Although this short treatment course at late-stage disease did not yield consistent changes in the frequencies of major lymphocyte subsets (Fig. S5H), it stimulated the activation and proliferation of multiple populations, with NK, NKT, and CD8 T cells all showing significant increases in Ki67 expression (Fig. 5I). The percentages of CD69$^+$ NK cells and granzyme B$^+$ CD8 T cells also tended to increase in DT-treated mice (Fig. S5I,J). Remarkably, MGL2$^+$ cell depletion also reduced the frequency of Foxp3$^+$ Treg by ~40% (Fig. 5J) and nearly doubled the CD8:Treg ratio (Fig. 5K).

CD11b$^+$ DC selectively inhibit CD8 T cell-mediated tumor immunity through PD-L2

These studies suggest that CD11b$^+$ DC promote metastasis by supporting Treg responses and suppressing various immune effector cells, but the molecular mechanisms responsible for their immunosuppressive effects remain unclear. Considering their expression of both PD-1 ligands (Fig. 2B,C) and evidence that these molecules suppress T cell responses *in vitro* (Fig. S4H), we wondered whether CD11b$^+$ DC utilize this particular pathway to regulate immune responses *in vivo*. Although less studied than PD-1 and PD-L1, we focused on the role of PD-L2, since its expression was also restricted to CD11b$^+$ DC in the liver of tumor-bearing mice (Fig. 2B,C and Fig. 6A,B). Furthermore, PD-L2 staining was largely restricted to CD11c$^+$ cells associated with metastases, whereas PD-L1 was also expressed in normal liver tissues (Fig. 6C).

We first tested the effects of PD-L2-blocking antibodies in the orthotopic model, allowing tumors to grow for 2 wk before beginning antibody treatment for 3 wk. Blocking PD-L2 did not affect primary tumor growth (Fig. S6A) but significantly reduced liver metastasis (Fig. 6D). Remarkably, many αPD-L2-treated mice with large primary tumors exhibited minimal metastatic disease, eliminating the correlation between primary tumor weight and metastatic burden observed in control mice (Fig. S6B). To determine whether these effects depend upon stimulation of tumor immunity, we analyzed immune cells in the liver after 10 d of treatment. Blocking PD-L2 did not significantly alter the frequencies of most major lymphocyte populations (Fig. 6E), including Foxp3$^+$ Treg (Fig. 6F), which is consistent with our *in vitro* studies. However, CD8 T cells tended to increase in αPD-L2-treated mice (Fig. 6E), resulting in a significant rise in the CD8:CD4 T cell ratio (Fig. 6G). Blocking PD-L2 increased the proliferation of CD8 T cells but not NK or CD4 T cells (Fig. 6H), further indicating selective activation of a CD8 T cell response. We obtained similar results in the experimental metastasis model, wherein mice began antibody treatment 1 wk following tumor injection (Fig. 6I). The trend toward reduced metastatic burden with αPD-L2 treatment was abolished in mice concomitantly treated with CD8 T cell-depleting antibodies (Fig. 6I), suggesting that the effects of PD-L2 blockade depend upon induction of CD8 T

cell-mediated tumor immunity. Altogether, these studies suggest that CD11b$^+$ DC protect developing metastases from immune attack by expanding Treg and suppressing CD8 T cells through a pathway involving PD-L2.

Similar DC accumulate at primary and secondary sites in other models and human PDAC

Extending these findings, MGL2$^+$ DC accumulated in and around liver metastases formed following i.s. injection of Panc02 cells (Fig. 7A) and in primary tumor tissues from a PDAC GEMM (*Pdx1-Cre*; *Kras$^{LSL\text{-}G12D/+}$*; *Cdkn2a$^{-/-}$*) (Fig. 7B). Moreover, we observed large numbers of CD11c$^+$HLA-DR$^+$ cells associated with human PDAC liver metastases (Fig. 7C), particularly at the leading edges where PD-L2$^+$ stromal cells were also abundant (Fig. S7A). In these same areas, we observed an accumulation of stromal cells expressing MGL (CLEC10A) (Fig. S7B), the human homolog of murine MGL1/2.

Further supporting our studies in the mouse model, gene expression levels of MGL and PD-L2 (*PDCD1LG2*) correlate with each other (Fig. 1D) and with CD11b (ITGAM), CD11c (*ITGAX*), HLA-DR (*HLA-DRA*), and the human DC marker DC-SIGN (*CD209*) in human PDAC tissues (Fig. 1E). Foxp3 (*FOXP3*) expression is also highly correlated with both MGL and PD-L2 (Fig. 1E), suggesting that analogous DC may support Treg responses in human PDAC. Consistent with the development of CD11b$^+$ DC in the mouse model, expression levels of MGL/PD-L2 correlate with Mo markers (*CCR2*, *CD14, CSF1R*), PD-L1 (*CD274*), GM-CSF (*CSF2*) and its receptor (*CSFR2A/B*), and the transcription factor IRF4 (*IRF4*), which was shown to regulate the development of MGL2$^+$PD-L2$^+$CD11b$^+$ DC in normal (48) and tumor (41) tissues. Altogether, these data suggest that immunosuppressive DC derived from Mo are involved in PDAC progression in multiple mouse models as well as the human disease.

Discussion

The prognosis for PDAC patients remains dismal (1, 2), largely due to presentation with inoperable locally advanced or metastatic disease as well as high rates of recurrence following surgery, especially at distant sites (3-5). Recent studies have begun to clarify how the immune system affects PDAC progression at the primary site (16-24). However, fewer have investigated the immune response associated with metastasis development at secondary sites. When studied, Mφ or Gr1$^+$ myeloid cells have been emphasized in this process (24-28), similar to reports in other models (7, 8, 34, 35). While also finding that these cells accumulate at metastatic sites, we were surprised to find that early metastases are enriched with a population of CD11b$^+$ DC. However, rather than stimulating immunosurveillance mechanisms that suppress tumor spread, these antigen-presenting cells facilitate metastasis by generating an immunosuppressive microenvironment that is enriched with Treg and by inhibiting CD8 T cell responses (Fig. S8A).

These findings were enabled by the highly restricted expression of both MGL2 and PD-L2 to CD11b$^+$ DC in the metastatic microenvironment. Indeed, we show here for the first time that PDAC metastasis is reduced by depleting a specific DC subset on the basis of MGL2 expression or by blocking PD-L2 (Fig. S8B,C). Consistent with our studies, coexpression of MGL2/CD301b and PD-L2 has been found to characterize IRF4-dependent CD11b$^+$ DC in

both normal (39, 48) and tumor (41) tissues. The effects observed upon $MGL2^+$ cell depletion or PD-L2 blockade support our *in vitro* studies showing that $CD11b^+$ DC preferentially induce Treg proliferation and impair CD8 T cell responses. Although our results suggest that multiple mechanisms may contribute to the anti-metastatic effects of $MGL2^+$ cell depletion, our studies with PD-L2-blocking antibodies indicate that the DC utilize this specific pathway to suppress CD8 T cell-mediated tumor immunity. We also show that these DC strongly stimulate Treg responses, but whether there exist mechanisms that can be targeted to selectively disrupt this interaction remains to be determined. The NK/NKT cell activation observed following $MGL2^+$ cell depletion suggests that $CD11b^+$ DC suppress these lymphocyte populations through pathways that remain to be identified as well. Finally, while our results collectively suggest that $CD11b^+$ DC facilitate metastasis by directly suppressing immune responses in the metastatic microenvironment, we cannot exclude a role in our studies for $MGL2^+$ and/or $PD\text{-}L2^+$ DC that reside in lymph nodes or other tissues apart from the metastatic site (39, 48).

Poor outcomes are associated with high Treg and low CD8 T cell infiltration in many cancers (11, 12), including PDAC (13-15). Our studies suggest that a specific DC subset supports both arms of this unfavorable immune response at metastatic sites, highlighting the therapeutic potential of targeting such cells to inhibit PDAC progression. Although our studies focus on the role of $CD11b^+$ DC at secondary sites, these cells also infiltrate primary tumors and thus may play a role in PDAC initiation and progression at the primary site. Our results reinforce the pathophysiological function of tumor-derived GM-CSF in PDAC (16, 17) and potentially other GM-CSF-producing cancers (49), finding that it drives $Gr1^+/Ly6C^+$ Mo to differentiate into $CD11b^+$ DC that express PD-1 ligands and expand Treg. Consistent with these findings, expression levels of MGL and PD-L2 correlate with DC markers, Foxp3, and GM-CSF and its receptor in human PDAC specimens. Recent studies in other models have shown that $Gr1^+/Ly6C^+$ Mo predominantly differentiate into Mφ-like cells that express CD64 and/or F4/80 at primary and metastatic sites (35, 36, 42). However, our studies show that $Gr1^+/Ly6C^+$ Mo exhibit a distinct differentiation pattern in PDAC metastasis, developing into cells that express low levels of the Mo/Mφ markers CD64, F4/80, and Gr1/Ly6C, and high levels of the DC markers CD11c, MHC-II, and CD24. We suspect that these differences are driven by the cytokine milieu encountered by infiltrating Mo, with the relative levels of M-CSF, GM-CSF, and potentially other factors (e.g. Flt3L) determining whether Mo develop into cells more closely resembling Mφ or DC (50). Supporting this, $MGL2^+CD11b^+$ DC accumulate in metastatic liver following injection of GM-CSF-producing PDAC cells but not tumor lines characterized by low GM-CSF production (B16, LLC, and MC38). Furthermore, PDAC supernatants stimulate DC differentiation and expression of both MGL2 and PD-L2 by Mo in a GM-CSF-dependent manner. Interestingly, MC38 also induces an infiltration of $CD11b^+$ DC-like cells, but these cells express low levels of MGL2 compared to PDAC-associated $CD11b^+$ DC, suggesting that alternative factors drive their development. Based on a recent study of the tumor-associated DC compartment (42), we suspect that these cells share a monocytic lineage but undergo a distinct differentiation program, resulting in a more Mo/Mφ-like phenotype characterized by Ly6C and CD64 expression. Viewed in this context, our studies underscore

the diversity of Mo differentiation patterns in cancer as well as the critical role of the tumor microenvironment in this process.

Our findings are consistent with a recent study that partitioned the tumor myeloid compartment into discrete DC and macrophage populations, and showed an essential role for CD11b$^-$ (CD103$^+$) DC in CD8 T cell-mediated tumor immunity (41). A CD11b$^+$ DC population dependent on GM-CSF signaling was identified in the same study, but its effects on tumor immunity and disease progression were not determined. Aligning with our own studies, the CD11b$^+$ DC population expanded in response to tumoral GM-CSF production and uniquely expressed both MGL2 and PD-L2. Leveraging the selective expression of these molecules, we show here that CD11b$^+$ DC represent the functional antithesis of tumor immunity-inducing CD11b$^-$ DC, as they both directly suppress CD8 T cells and expand Treg in the metastatic microenvironment. Correspondingly, depleting or blocking the activity of the CD11b$^+$ DC subset stimulates antitumor immune responses and suppresses metastasis development. The drastic shift toward CD11b$^+$ DC that occurs at secondary sites in our model is consistent with this functional dichotomy and may be essential for the evasion of immunosurveillance mechanisms that would block metastasis formation. The antitumor T cell response induced by CD11b$^+$ DC depletion suggests that this approach could also make tumors more responsive to other immunotherapies, including T cell-directed checkpoint blockers and agonistic antibodies. However, the optimal molecular target for depletion of this DC subset in human cancer remains unclear, as human MGL is also expressed in a number of normal tissues (proteinatlas.org). More broadly, our findings highlight the heterogeneity of the tumor-associated myeloid response and suggest that myeloid cell-directed immunotherapies need to be tailored to different cancers. Ultimately, effective management of the tumor myeloid compartment may require multiple interventions, with efforts aimed at both expanding immunostimulatory cell populations (e.g. CD103$^+$ DC) and depleting or modulating immunosuppressive ones (e.g. CD11b$^+$ DC, TAM, and/or MDSC). Our studies contribute to this latter goal and suggest multiple ways of targeting an abundant, immunosuppressive DC population for therapeutic effect in pancreatic cancer.

Supplementary Material

Refer to Web version on PubMed Central for supplementary material.

Acknowledgments

We are grateful to Dr. Michael Bachmann for assistance with tumor cell-labeling, Drs. Brendan Visser and Moe Jalali for help in obtaining human specimens, and Dr. Akiko Iwasaki for providing the *Mgl2*^{DTR} mice. We also thank past and present members of the Engleman lab for their assistance and feedback, especially Xianne Penny, Michael Alonso, Lei Shen, Claudia Benike, Tyler Prestwood, Yaron Carmi, and Robert Yuan.

Financial Support: This work was supported by NIH grants R01 CA196657, U01 CA141468, and U54 CA209971 (E.G. Engleman); T32 AI007290 (J.A. Kenkel and M.G. Davidson); and F32 CA189408 (N.E. Reticker-Flynn).

References

1. Ryan DP, Hong TS, Bardeesy N. Pancreatic adenocarcinoma. N Engl J Med. 2014; 371(11):1039–49. [PubMed: 25207767]

2. Kamisawa T, Wood LD, Itoi T, Takaori K. Pancreatic cancer. Lancet. 2016; 388(10039):73–85. [PubMed: 26830752]
3. Paik KY, Choi SH, Heo JS, Choi DW. Analysis of liver metastasis after resection for pancreatic ductal adenocarcinoma. World J Gastrointest Oncol. 2012; 4(5):109–14. [PubMed: 22645634]
4. Van den Broeck A, Sergeant G, Ectors N, Van Steenbergen W, Aerts R, Topal B. Patterns of recurrence after curative resection of pancreatic ductal adenocarcinoma. Eur J Surg Oncol. 2009; 35(6):600–4. [PubMed: 19131205]
5. Katz MH, Wang H, Fleming JB, Sun CC, Hwang RF, Wolff RA, et al. Long-term survival after multidisciplinary management of resected pancreatic adenocarcinoma. Ann Surg Oncol. 2009; 16(4):836–47. [PubMed: 19194760]
6. Chang DT, Schellenberg D, Shen J, Kim J, Goodman KA, Fisher GA, et al. Stereotactic radiotherapy for unresectable adenocarcinoma of the pancreas. Cancer. 2009; 115(3):665–72. [PubMed: 19117351]
7. Sleeman JP. The metastatic niche and stromal progression. Cancer Metastasis Rev. 2012; 31(3-4): 429–40. [PubMed: 22699312]
8. Smith HA, Kang Y. The metastasis-promoting roles of tumor-associated immune cells. J Mol Med (Berl). 2013; 91(4):411–29. [PubMed: 23515621]
9. Schreiber RD, Old LJ, Smyth MJ. Cancer immunoediting: integrating immunity's roles in cancer suppression and promotion. Science. 2011; 331(6024):1565–70. [PubMed: 21436444]
10. Colotta F, Allavena P, Sica A, Garlanda C, Mantovani A. Cancer-related inflammation, the seventh hallmark of cancer: links to genetic instability. Carcinogenesis. 2009; 30(7):1073–81. [PubMed: 19468060]
11. Fridman WH, Pages F, Sautes-Fridman C, Galon J. The immune contexture in human tumours: impact on clinical outcome. Nat Rev Cancer. 2012; 12(4):298–306. [PubMed: 22419253]
12. Gooden MJ, de Bock GH, Leffers N, Daemen T, Nijman HW. The prognostic influence of tumour-infiltrating lymphocytes in cancer: a systematic review with meta-analysis. Br J Cancer. 2011; 105(1):93–103. [PubMed: 21629244]
13. Hiraoka N, Onozato K, Kosuge T, Hirohashi S. Prevalence of FOXP3+ regulatory T cells increases during the progression of pancreatic ductal adenocarcinoma and its premalignant lesions. Clin Cancer Res. 2006; 12(18):5423–34. [PubMed: 17000676]
14. Ino Y, Yamazaki-Itoh R, Shimada K, Iwasaki M, Kosuge T, Kanai Y, et al. Immune cell infiltration as an indicator of the immune microenvironment of pancreatic cancer. Br J Cancer. 2013; 108(4): 914–23. [PubMed: 23385730]
15. Tewari N, Zaitoun AM, Arora A, Madhusudan S, Ilyas M, Lobo DN. The presence of tumour-associated lymphocytes confers a good prognosis in pancreatic ductal adenocarcinoma: an immunohistochemical study of tissue microarrays. BMC Cancer. 2013; 13:436. [PubMed: 24063854]
16. Bayne LJ, Beatty GL, Jhala N, Clark CE, Rhim AD, Stanger BZ, et al. Tumor-derived granulocyte-macrophage colony-stimulating factor regulates myeloid inflammation and T cell immunity in pancreatic cancer. Cancer Cell. 2012; 21(6):822–35. [PubMed: 22698406]
17. Pylayeva-Gupta Y, Lee KE, Hajdu CH, Miller G, Bar-Sagi D. Oncogenic Kras-induced GM-CSF production promotes the development of pancreatic neoplasia. Cancer Cell. 2012; 21(6):836–47. [PubMed: 22698407]
18. Ijichi H, Chytil A, Gorska AE, Aakre ME, Bierie B, Tada M, et al. Inhibiting Cxcr2 disrupts tumor-stromal interactions and improves survival in a mouse model of pancreatic ductal adenocarcinoma. J Clin Invest. 2011; 121(10):4106–17. 10.1172/JCI42754. [PubMed: 21926469]
19. Mitchem JB, Brennan DJ, Knolhoff BL, Belt BA, Zhu Y, Sanford DE, et al. Targeting tumor-infiltrating macrophages decreases tumor-initiating cells, relieves immunosuppression, and improves chemotherapeutic responses. Cancer Res. 2013; 73(3):1128–41. [PubMed: 23221383]
20. Stromnes IM, Brockenbrough JS, Izeradjene K, Carlson MA, Cuevas C, Simmons RM, et al. Targeted depletion of an MDSC subset unmasks pancreatic ductal adenocarcinoma to adaptive immunity. Gut. 2014; 63(11):1769–81. [PubMed: 24555999]

21. Zhang Y, Yan W, Mathew E, Bednar F, Wan S, Collins MA, et al. CD4+ T lymphocyte ablation prevents pancreatic carcinogenesis in mice. Cancer Immunol Res. 2014; 2(5):423–35. [PubMed: 24795355]
22. McAllister F, Bailey JM, Alsina J, Nirschl CJ, Sharma R, Fan H, et al. Oncogenic Kras activates a hematopoietic-to-epithelial IL-17 signaling axis in preinvasive pancreatic neoplasia. Cancer Cell. 2014; 25(5):621–37. [PubMed: 24823639]
23. Lesina M, Kurkowski MU, Ludes K, Rose-John S, Treiber M, Kloppel G, et al. Stat3/Socs3 activation by IL-6 transsignaling promotes progression of pancreatic intraepithelial neoplasia and development of pancreatic cancer. Cancer Cell. 2011; 19(4):456–69. [PubMed: 21481788]
24. Sanford DE, Belt BA, Panni RZ, Mayer A, Deshpande AD, Carpenter D, et al. Inflammatory monocyte mobilization decreases patient survival in pancreatic cancer: a role for targeting the CCL2/CCR2 axis. Clin Cancer Res. 2013; 19(13):3404–15. [PubMed: 23653148]
25. Connolly MK, Mallen-St Clair J, Bedrosian AS, Malhotra A, Vera V, Ibrahim J, et al. Distinct populations of metastases-enabling myeloid cells expand in the liver of mice harboring invasive and preinvasive intra-abdominal tumor. J Leukoc Biol. 2010; 87(4):713–25. [PubMed: 20042467]
26. Steele CW, Karim SA, Leach JD, Bailey P, Upstill-Goddard R, Rishi L, et al. CXCR2 Inhibition Profoundly Suppresses Metastases and Augments Immunotherapy in Pancreatic Ductal Adenocarcinoma. Cancer Cell. 2016; 29(6):832–45. [PubMed: 27265504]
27. Nielsen SR, Quaranta V, Linford A, Emeagi P, Rainer C, Santos A, et al. Macrophage-secreted granulin supports pancreatic cancer metastasis by inducing liver fibrosis. Nat Cell Biol. 2016; 18(5):549–60. [PubMed: 27088855]
28. Costa-Silva B, Aiello NM, Ocean AJ, Singh S, Zhang H, Thakur BK, et al. Pancreatic cancer exosomes initiate pre-metastatic niche formation in the liver. Nat Cell Biol. 2015; 17(6):816–26. [PubMed: 25985394]
29. Brahmer JR, Tykodi SS, Chow LQ, Hwu WJ, Topalian SL, Hwu P, et al. Safety and activity of anti-PD-L1 antibody in patients with advanced cancer. N Engl J Med. 2012; 366(26):2455–65. [PubMed: 22658128]
30. Le DT, Lutz E, Uram JN, Sugar EA, Onners B, Solt S, et al. Evaluation of ipilimumab in combination with allogeneic pancreatic tumor cells transfected with a GM-CSF gene in previously treated pancreatic cancer. J Immunother. 2013; 36(7):382–9. [PubMed: 23924790]
31. Westphalen CB, Olive KP. Genetically engineered mouse models of pancreatic cancer. Cancer J. 2012; 18(6):502–10. [PubMed: 23187836]
32. Herreros-Villanueva M, Hijona E, Cosme A, Bujanda L. Mouse models of pancreatic cancer. World J Gastroenterol. 2012; 18(12):1286–94. [PubMed: 22493542]
33. Tseng WW, Winer D, Kenkel JA, Choi O, Shain AH, Pollack JR, et al. Development of an orthotopic model of invasive pancreatic cancer in an immunocompetent murine host. Clin Cancer Res. 2010; 16(14):3684–95. [PubMed: 20534740]
34. Kowanetz M, Wu X, Lee J, Tan M, Hagenbeek T, Qu X, et al. Granulocyte-colony stimulating factor promotes lung metastasis through mobilization of Ly6G+Ly6C+ granulocytes. Proc Natl Acad Sci U S A. 2010; 107(50):21248–55. [PubMed: 21081700]
35. Qian BZ, Li J, Zhang H, Kitamura T, Zhang J, Campion LR, et al. CCL2 recruits inflammatory monocytes to facilitate breast-tumour metastasis. Nature. 2011; 475(7355):222–5. [PubMed: 21654748]
36. Qian B, Deng Y, Im JH, Muschel RJ, Zou Y, Li J, et al. A distinct macrophage population mediates metastatic breast cancer cell extravasation, establishment and growth. PLoS One. 2009; 4(8):e6562. [PubMed: 19668347]
37. Hingorani SR, Wang L, Multani AS, Combs C, Deramaudt TB, Hruban RH, et al. Trp53R172H and KrasG12D cooperate to promote chromosomal instability and widely metastatic pancreatic ductal adenocarcinoma in mice. Cancer Cell. 2005; 7(5):469–83. [PubMed: 15894267]
38. Hackett PB, Ekker SC, Largaespada DA, McIvor RS. Sleeping beauty transposon-mediated gene therapy for prolonged expression. Adv Genet. 2005; 54:189–232. [PubMed: 16096013]
39. Kumamoto Y, Linehan M, Weinstein JS, Laidlaw BJ, Craft JE, Iwasaki A. CD301b(+) dermal dendritic cells drive T helper 2 cell-mediated immunity. Immunity. 2013; 39(4):733–43. [PubMed: 24076051]

40. Merad M, Sathe P, Helft J, Miller J, Mortha A. The dendritic cell lineage: ontogeny and function of dendritic cells and their subsets in the steady state and the inflamed setting. Annu Rev Immunol. 2013; 31:563–604. [PubMed: 23516985]
41. Broz ML, Binnewies M, Boldajipour B, Nelson AE, Pollack JL, Erle DJ, et al. Dissecting the tumor myeloid compartment reveals rare activating antigen-presenting cells critical for T cell immunity. Cancer Cell. 2014; 26(5):638–52. [PubMed: 25446897]
42. Laoui D, Keirsse J, Morias Y, Van Overmeire E, Geeraerts X, Elkrim Y, et al. The tumour microenvironment harbours ontogenically distinct dendritic cell populations with opposing effects on tumour immunity. Nat Commun. 2016; 7:13720. [PubMed: 28008905]
43. Grivennikov SI, Karin M. Inflammatory cytokines in cancer: tumour necrosis factor and interleukin 6 take the stage. Ann Rheum Dis. 2011; 70(Suppl 1):i104–8. [PubMed: 21339211]
44. Shevach EM, Tran DQ, Davidson TS, Andersson J. The critical contribution of TGF-beta to the induction of Foxp3 expression and regulatory T cell function. Eur J Immunol. 2008; 38(4):915–7. [PubMed: 18395859]
45. Thornton AM, Korty PE, Tran DQ, Wohlfert EA, Murray PE, Belkaid Y, et al. Expression of Helios, an Ikaros transcription factor family member, differentiates thymic-derived from peripherally induced Foxp3+ T regulatory cells. J Immunol. 2010; 184(7):3433–41. [PubMed: 20181882]
46. Zou T, Caton AJ, Koretzky GA, Kambayashi T. Dendritic cells induce regulatory T cell proliferation through antigen-dependent and -independent interactions. J Immunol. 2010; 185(5): 2790–9. [PubMed: 20686126]
47. Kim JM, Rasmussen JP, Rudensky AY. Regulatory T cells prevent catastrophic autoimmunity throughout the lifespan of mice. Nat Immunol. 2007; 8(2):191–7. [PubMed: 17136045]
48. Gao Y, Nish SA, Jiang R, Hou L, Licona-Limon P, Weinstein JS, et al. Control of T helper 2 responses by transcription factor IRF4-dependent dendritic cells. Immunity. 2013; 39(4):722–32. [PubMed: 24076050]
49. Hong IS. Stimulatory versus suppressive effects of GM-CSF on tumor progression in multiple cancer types. Exp Mol Med. 2016; 48(7):e242. [PubMed: 27364892]
50. Van Overmeire E, Stijlemans B, Heymann F, Keirsse J, Morias Y, Elkrim Y, et al. M-CSF and GM-CSF Receptor Signaling Differentially Regulate Monocyte Maturation and Macrophage Polarization in the Tumor Microenvironment. Cancer Res. 2016; 76(1):35–42. [PubMed: 26573801]

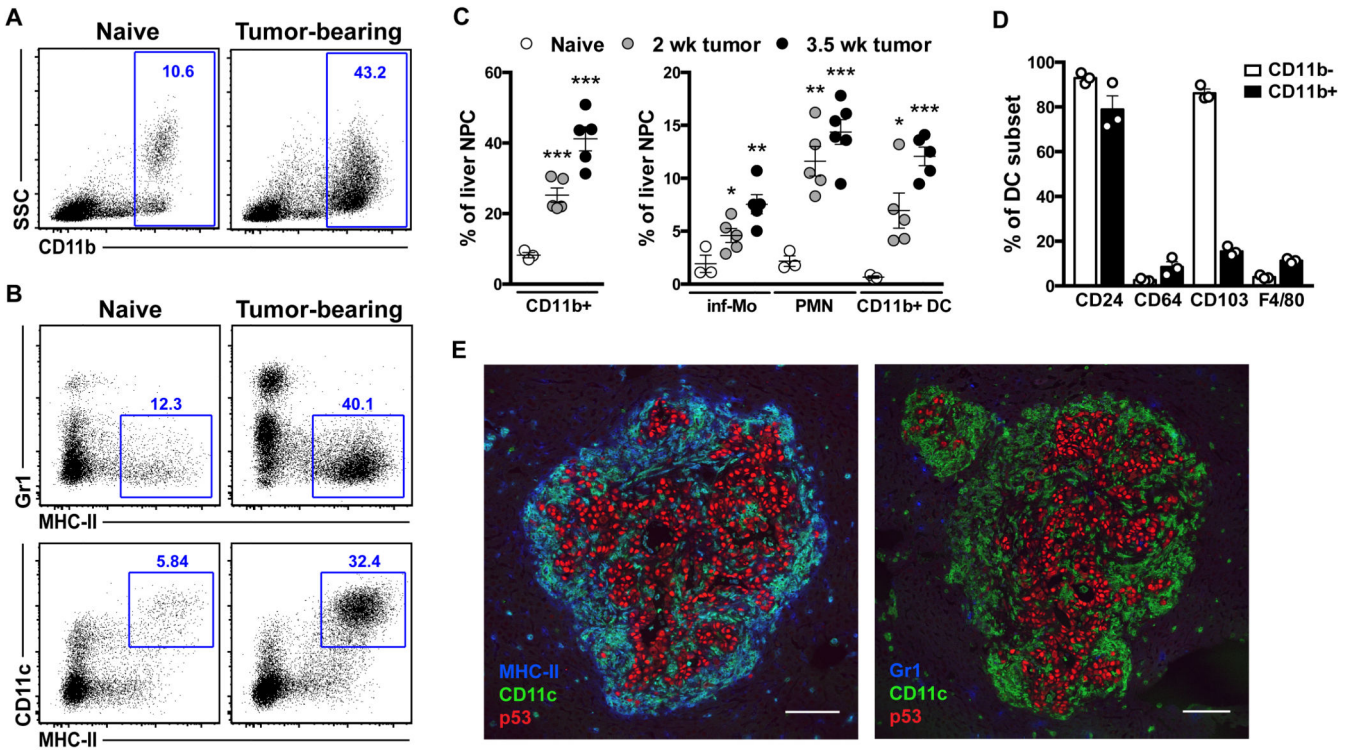

Figure 1. CD11b$^+$ DC accumulate at secondary sites and surround early metastases

(A-C) Liver non-parenchymal cells (NPC) were analyzed by flow cytometry at the indicated time points following pancreatic tumor implantation or 2 wk after sham operation for naïve mice. (A, B) Representative plots depicting total CD11b$^+$ cells among NPC (A) and markers expressed by CD11b$^+$ cells from naïve and 3.5 wk tumor-bearing mice (B). (C) Frequencies of CD11b$^+$ cells and subsets in naïve and tumor-bearing mice with means ± SEM shown. (D) Marker expression by CD11b$^-$ and CD11b$^+$ DC (CD11c^{hi}MHC-II^{hi}) subsets from tumor-bearing mice with means ± SEM shown. (E) Micrometastatic liver sections stained with the indicated antibodies. Tumor cells are marked by the accumulation of mutant p53. Scale bar, 100 μm. *, p<0.05; **, p<0.01; ***, p<0.001 by Student's *t*-test comparing tumor-bearing to naïve mice. See also Fig. S1.

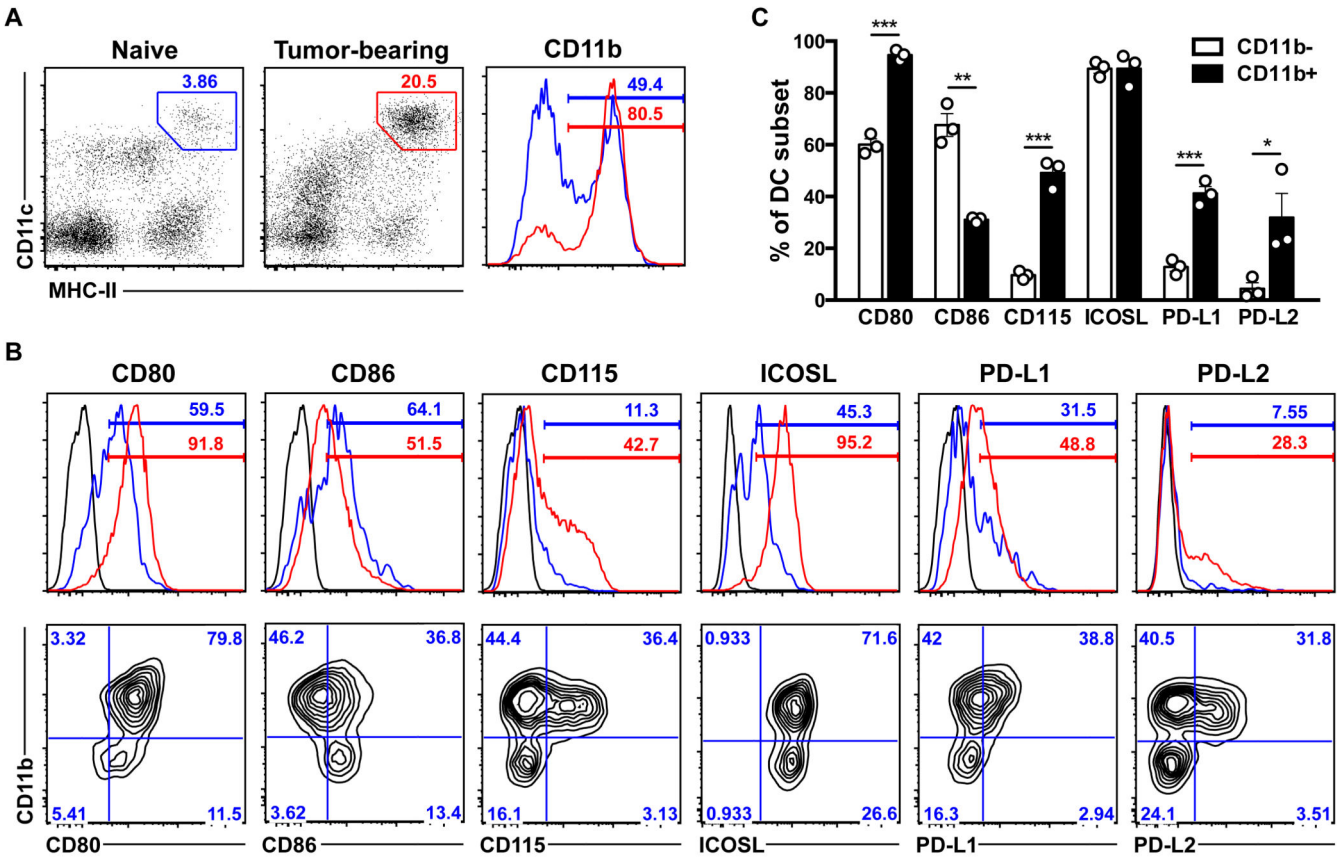

Figure 2. CD11b^{+} DC selectively expand at secondary sites and exhibit immunosuppressive features

(A-C) Total CD11c^{hi}MHC-II^{hi} DC of CD45^{+} liver NPC from naïve (blue) and tumor-bearing (red) mice were analyzed for the expression of the indicated markers. Histograms depict expression by total liver DC (A, B) and plots show expression by CD11b^{-} and CD11b^{+} subsets from tumor-bearing mice (B, bottom panel). (C) Marker expression by DC subsets from tumor-bearing mice with means ± SEM shown. *, p<0.05; **, p<0.01; ***, p<0.001 by Student's *t*-test.

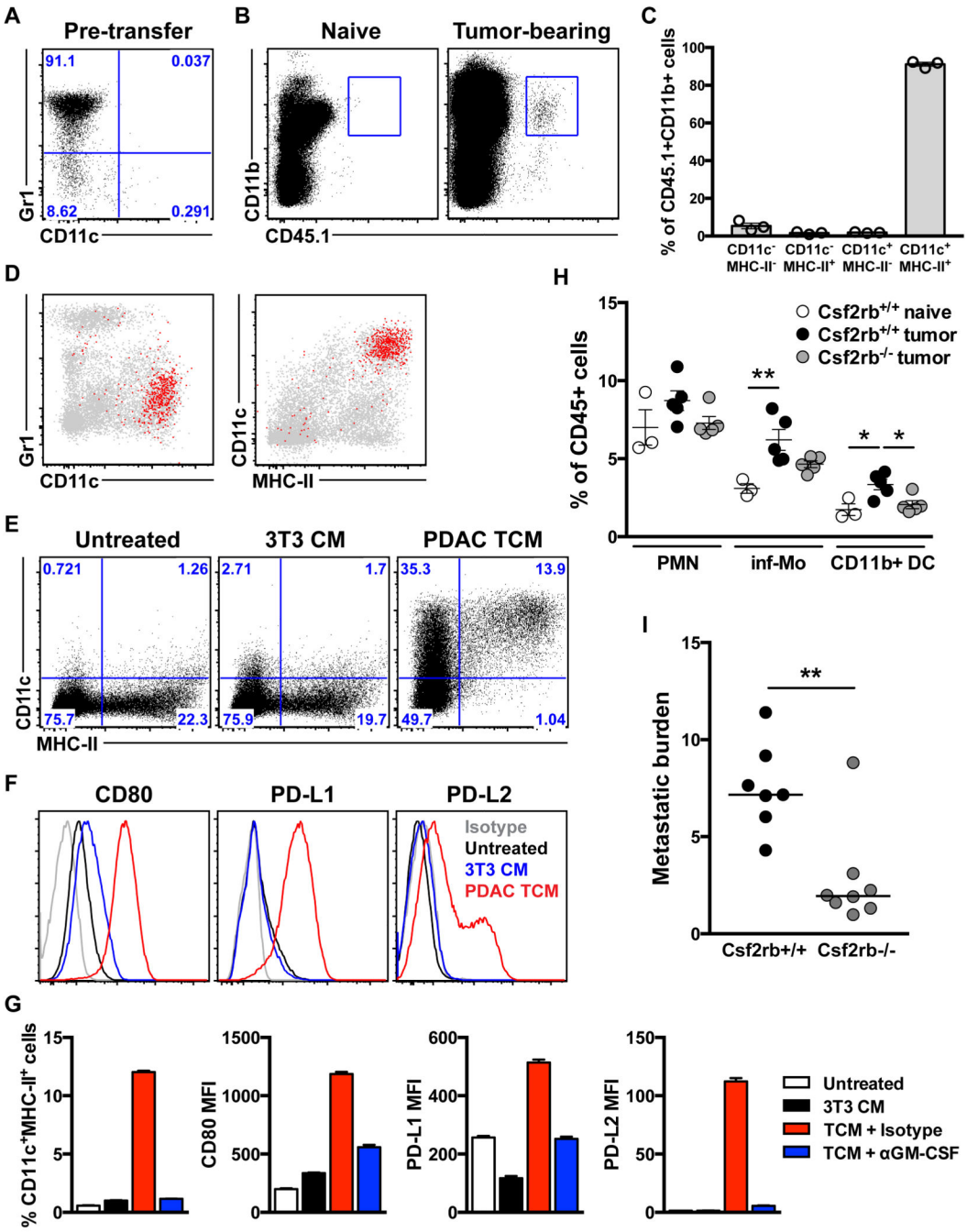

Figure 3. Metastasis-associated CD11b$^+$ DC develop from monocytes in response to tumor-released GM-CSF

(A-D) BM Mo from naïve CD45.1×129 F1 mice were transferred into naïve or 3.5 wk tumor-bearing mice and analyzed by flow cytometry after 5 d. (A) Phenotype of BM Mo prior to transfer. (B) Plots depicting recovery of donor-derived cells from the livers of tumor-bearing but not naïve mice. (C, D) Phenotype of CD45.1$^+$CD11b$^+$ cells (red) overlaid on host hematopoietic cells (gray) (D) and percentages of donor cells displaying the indicated phenotype with means ± SEM shown (C). (E-G) BM Mo from naïve mice were cultured for 18-24 hr in the presence of control or conditioned media ± the indicated antibodies, and then

total $CD11b^+$ cells were analyzed for the expression of the indicated markers. (H, I) BM chimeras were generated using WT ($Csf2rb^{+/+}$) or GM-CSFR KO ($Csf2rb^{-/-}$) donor cells and used in the experimental liver metastasis model. (H) $CD11b^+$ subset frequencies in the liver 12 d after sham operation or tumor cell injection with means ± SEM shown. (I) Metastatic burden 21 d following tumor cell injection with medians shown. *, $p<0.05$; **, $p<0.01$ by one-way ANOVA with *post hoc* Tukey's test (H) or Mann-Whitney *U*-test (I). See also Fig. S2.

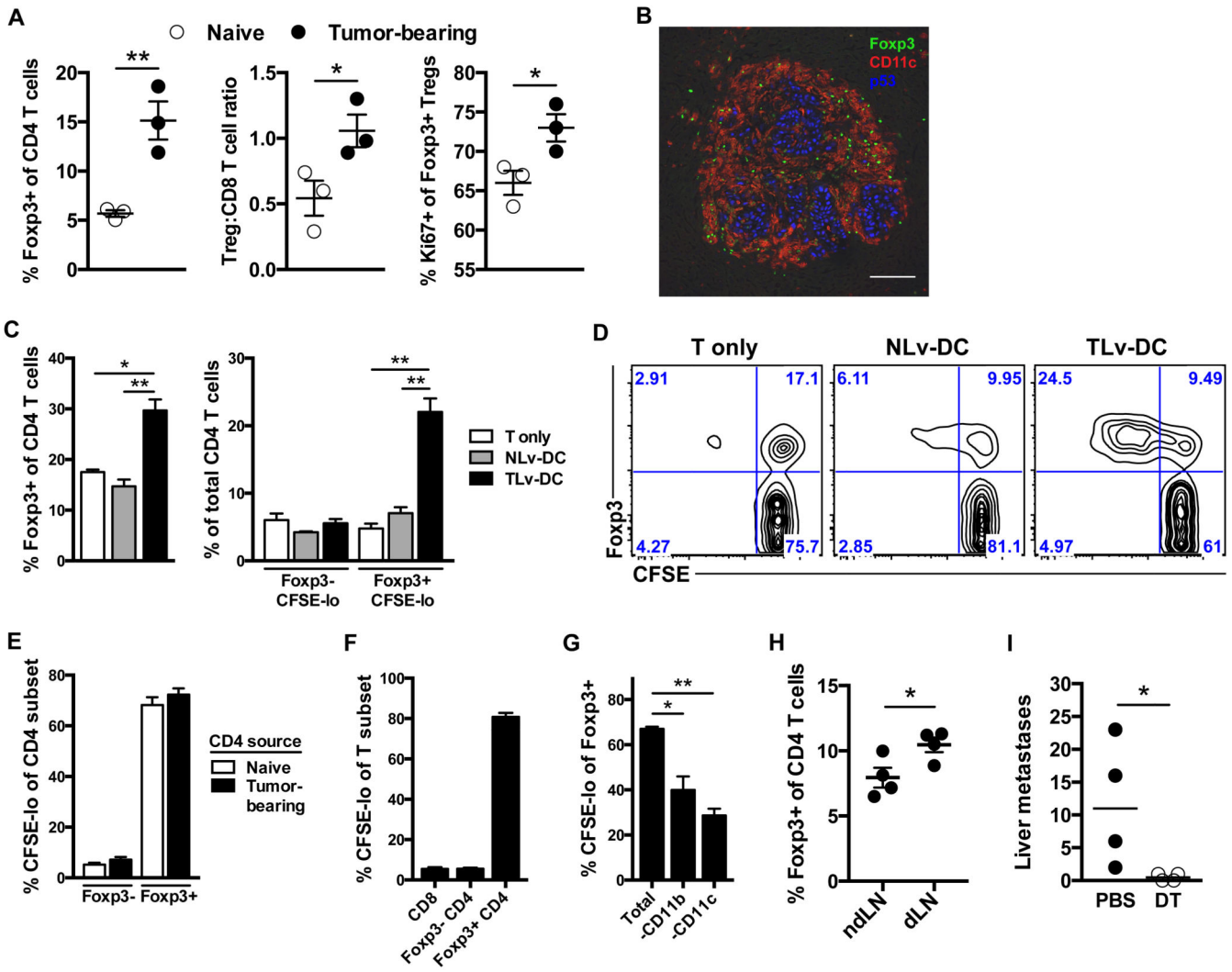

Figure 4. Treg expansion supported by CD11b$^+$ DC facilitates metastasis development

(A) T cells from the liver of naïve and 4 wk tumor-bearing mice were analyzed by flow cytometry. Means ± SEM of cells with indicated phenotype and of cell ratios are shown. (B) Micrometastatic liver tissue section stained with the indicated antibodies. Scale bar, 100 μm. (C, D) CFSE-labeled CD4 T cells from naïve mice were cultured alone or with liver DC from naïve (NLv-DC) or tumor-bearing (TLv-DC) mice and analyzed by flow cytometry after 3-4 d. Results depicted are representative of >5 independent experiments. Mean frequencies ± SEM of cells with indicated phenotypes in separate cultures (n=3-5) are shown in all bar graphs within this figure. (E) Division of CD4 T cells obtained from naïve or tumor-bearing mice following coculture with TLv-DC. (F) Division rates among T cell populations following coculture of TLv-DC with pan T cells from tumor-bearing mice. (G) Treg division in cultures of total liver NPC from tumor-bearing mice, depleted or not of CD11b$^+$ or CD11c$^+$ cells. (H) Foxp3$^+$ Treg among CD4 T cells from draining and non-draining popliteal lymph nodes (n=4 pooled samples/group) 3 d following footpad injection of TLv-DC, with means ± SEM shown. (I) Spontaneous liver metastases with medians shown for *Foxp3^{DTR}* hosts treated with PBS or DT. *, p<0.05; **, p<0.01; ***, p<0.001;

****, p<0.0001 by Student's *t*-test (A, H), one-way ANOVA with *post hoc* Tukey's test (C, G), or Mann-Whitney *U*-test (I). See also Fig. S3 and Fig. S4.

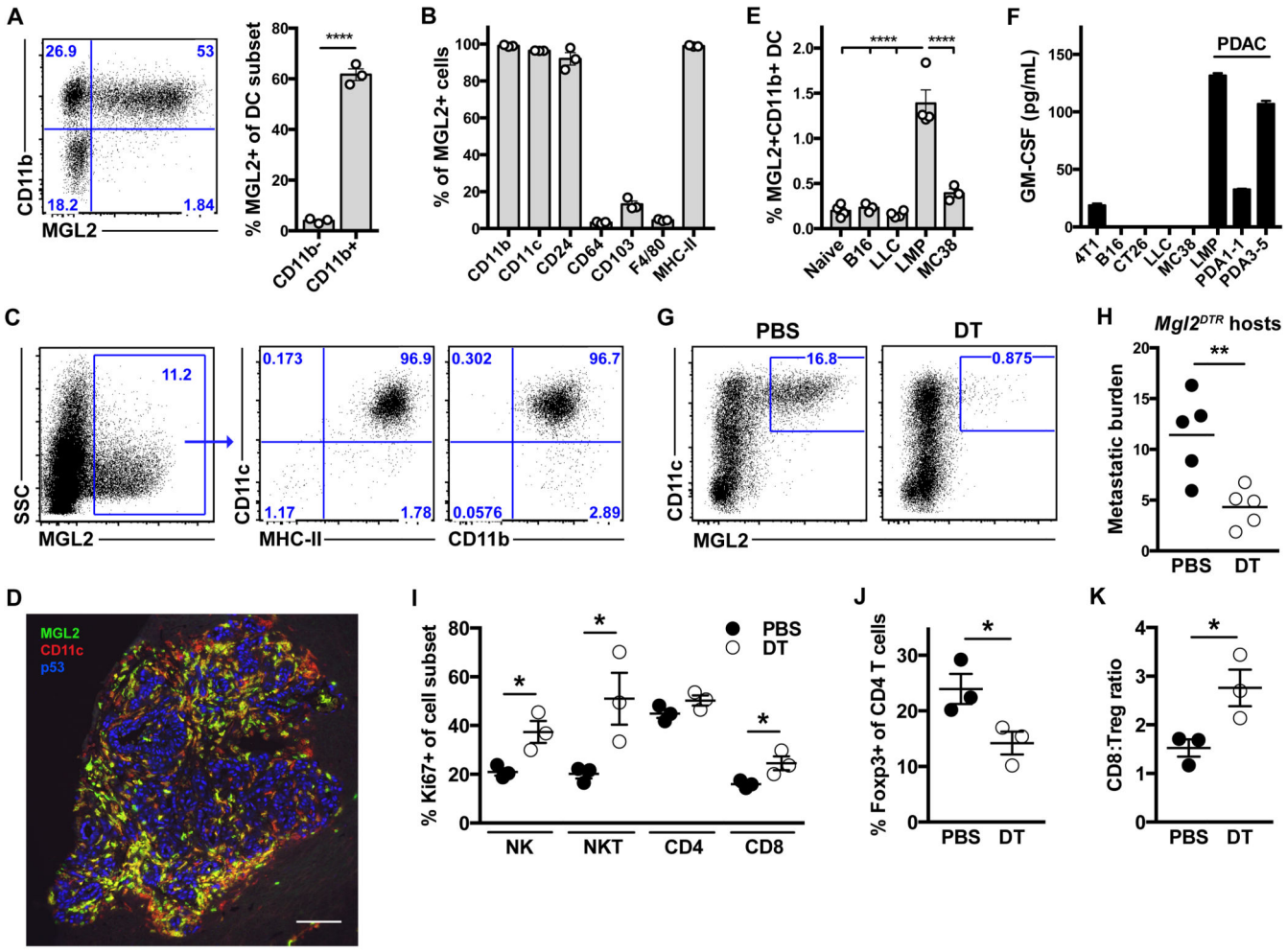

Figure 5. MGL2-expessing CD11b$^+$ DC suppress cytotoxic lymphocytes, expand Treg, and promote metastasis

(A) MGL2 expression by DC subsets from the liver of tumor-bearing mice with means ± SEM shown. (B, C) Phenotypic analysis of total MGL2$^+$CD45$^+$ cells, including representative plots (C) and summary of marker expression with means ± SEM shown (B). (D) Micrometastatic liver tissue section obtained 15 d following intrasplenic tumor cell injection and stained with the indicated antibodies. Scale bar, 100 μm. (E) MGL2$^+$CD11b$^+$CD11c$^+$MHC-II$^+$ cells among CD45$^+$ NPC from naïve mice or 14 d following i.s. tumor cell injection, with means ± SEM shown. (F) GM-CSF levels in tumor cell supernatants following 24 hr culture. (G-K) *Mgl2^{DTR}* mice in the experimental metastasis model were treated with PBS or DT beginning on d10 (H) or d20 (G, I-K) following tumor injection. (G) MGL2$^+$CD11c$^+$ cells among CD45$^+$ NPC are gated. (H) Metastatic burden 25 d following tumor cell injection with means shown. (I-K) Means ± SEM of cells expressing indicated marker or of cell ratios. Results shown are representative of two independent experiments with similar results. *, p<0.05; **, p<0.01; ****, p<0.0001 by Student's *t*-test (A, H, I, J, K) or one-way ANOVA with *post hoc* Tukey's test (E). See also Fig. S5.

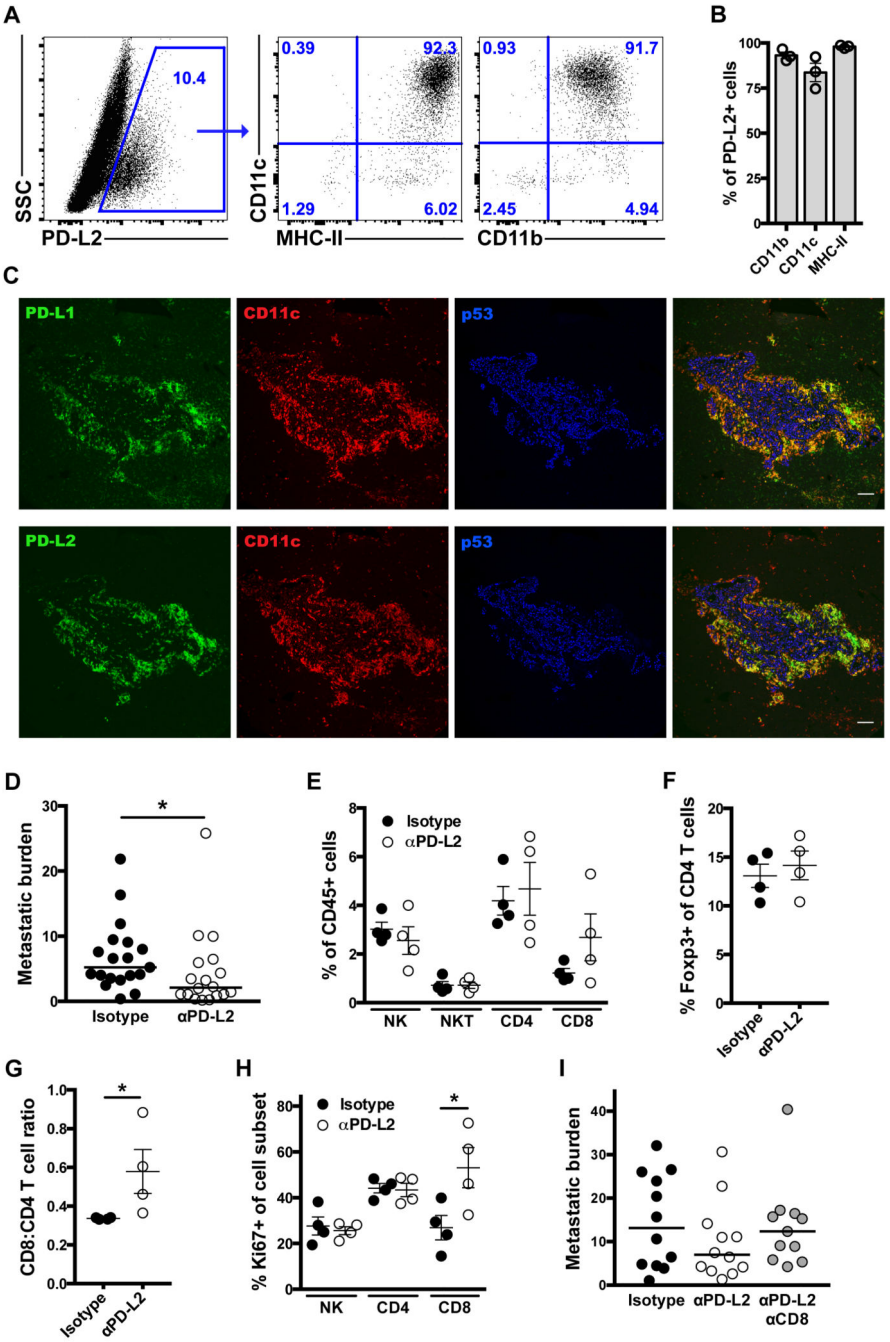

Figure 6. CD11b^{+} DC inhibit CD8 T cell-mediated tumor immunity through PD-L2

(A, B) Total PD-L2^{+}CD45^{+} cells from micrometastatic liver are gated (A) and their phenotype displayed (A, B), with means ± SEM shown. (C) Micrometastatic liver tissue sections stained with the indicated antibodies. Scale bar, 100 μm. (D) Metastatic burden with medians shown for orthotopic tumor-bearing mice treated with the indicated antibodies. (E-H) Means ± SEM of cells with indicated phenotypes and cell ratios after 10 d of antibody treatment. (I) Metastatic burden with medians shown for mice treated with indicated

antibodies following intrasplenic tumor cell injection. *, $p<0.05$ by Mann-Whitney *U*-test (D, G) or Student's *t*-test (H). See also Fig. S6.

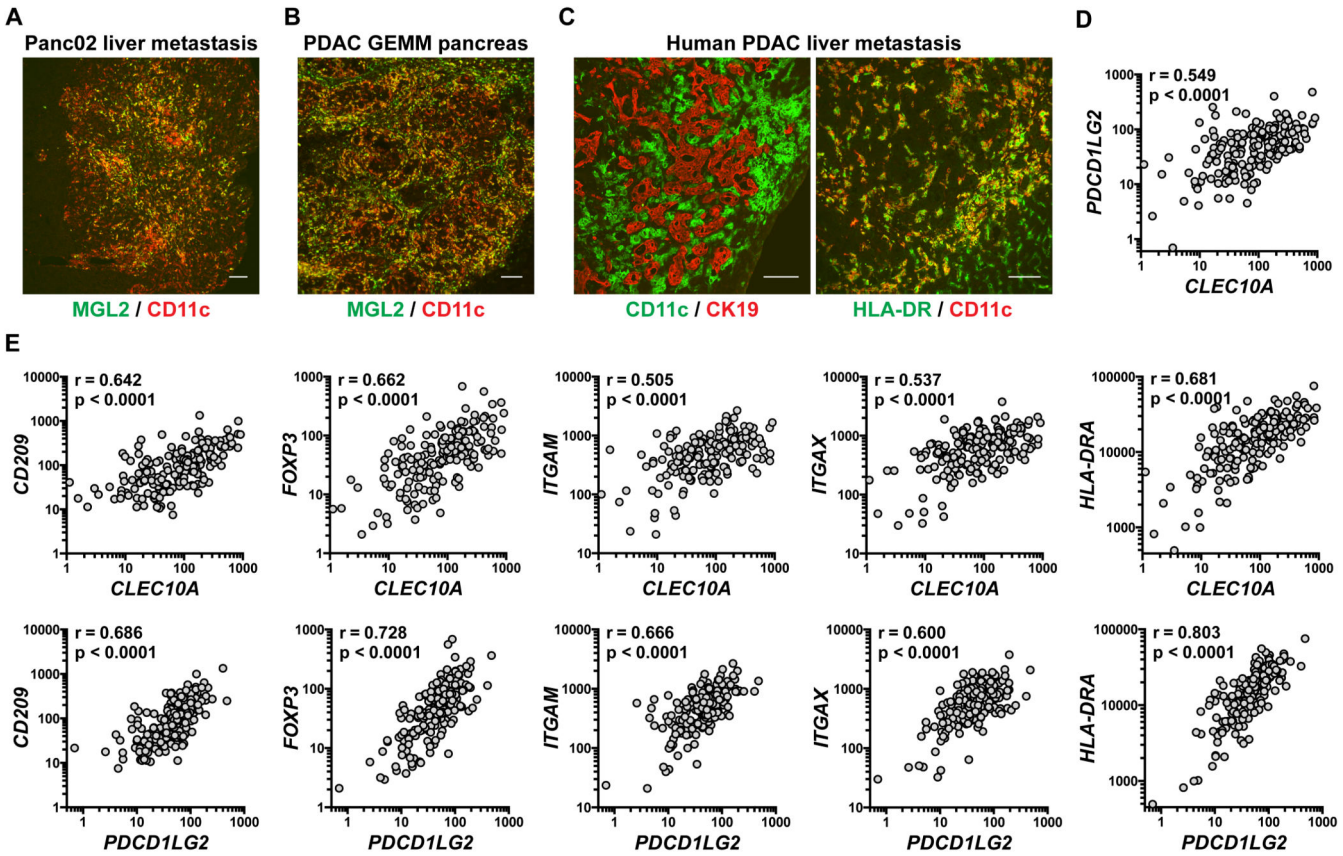

Figure 7. Similar DC accumulate at primary and secondary sites in other models and human PDAC

(A-C) Tissue sections stained with the indicated antibodies and obtained from (A) mouse 20 d after i.s. injection of Panc02 cells, (B) 8-wk-old *Pdx1-Cre*; $Kras^{LSL\text{-}G12D/+}$; $Cdkn2a^{-/-}$ ($PK4^{-/-}$) mouse, or (C) PDAC patient. Scale bars, 100 μm. (D, E) Matched gene expression values (RSEM) for indicated gene pairs, obtained from the TCGA PDAC dataset (n=179). Spearman correlation coefficients and associated p-values are shown. See also Fig. S7.